SENRA Academic Publishers, Burnaby, British Columbia
Vol. 5, No. 1, pp. 1419-1428, Feb 2011
Online ISSN: 1920-3853; Print ISSN: 1715-9997

Canadian Journal of pure&applied sciences

ANALYSIS OF NET-SHAPE CLOSED-DIE SINTER-FORGING OF CENTRALLY LOCATED CYLINDRICAL PREFORMS

PC Sekhar[1] and *S Singh[2]
[1]School of Mechanical Engineering, KIIT University, Bhubaneswar-751024, Orissa
[2]School of Mechanical Engineering, KIIT University, Bhubaneswar-751024, Orissa, India

ABSTRACT

The present paper aims at studying the net-shape closed-die sinter-forging of centrally located cylindrical preforms within closed dies. The net-shape sinter-forging has been considered in two stages; where first stage consists of preform free barreling and the second stage consists of constraint deformation during which die corners are continuously formed and filled till the process is completed. The experiments were carried on a hydraulic press using closed-die set having upper and lower punches with centrally located cylindrical recess cavities having diameter equal to that of the cylindrical preforms, so that preforms can be loaded centrally with respect to the axis of the central container. Three separate modes of deformation were considered during the theoretical analysis using 'Upper Bound' approach, which were based on the different division of preform. The generalized expressions for the velocity field, strain rates, internal, frictional, inertia, energy dissipations and average forging loads have been formulated for each of these cases. The effect of die velocity, preform aspect ratio on energy dissipations, die cavity fills and die loads were investigated and results were verified experimentally and compared. It is expected that the present work will be useful for the analysis of net-shape forging of sintered materials.

Keywords: Net-Shape, upper bound, closed-die, sinter-forging.

Nomenclature

U_{ij}	velocity field	$\dot{\varepsilon}_{ij}$	strain rates
U	die velocity	$\dot{U}$	die acceleration
σ_0	flow stress of sintered material	n	constant greater than unity
P_{av}	average die pressure	F_{av}	average die load
A_{av}	average cross-sectional area	h	height of unfilled region
H_0	preform initial height	ρ_i	preform initial relative density
ρ_0	preform relative density	τ	interfacial frictional shear stress
W_i	internal energy dissipation	W_{f_1}	die-workpiece frictional energy dissipation
ξ	inertia factor	W_{f_2}	die-container frictional energy dissipation
ζ	load factor	W_a	inertia energy dissipation
J	total external energy supplied by press	R_0	flange radius
R'_0	hub radius	r_m	sticking zone radial distance
μ	coefficient of interfacial friction	ϕ_o	specific cohesion of contact area
η,	function of 'ρ_0'	Ψ	function of 'R_0'

Subscripts

r	radial	θ	circumferential	z	vertical

INTRODUCTION

Net-shape forging technology, which results into minimal material wastage, is the subject of much interest in the current industrial scenario mainly due to high yield by manufacture of the net-shape or near-net-shape components. This entails the use of completely or nearly completely closed cavity dies without drafts, normally on mechanical presses. Flash, which is the major form of metal wastage in the conventional forging, is thus eliminated (Thomson, 1986; Lee *et al*., 1997; Serdyuk *et al*., 2000). One of the major problems associated with the flashless or net-shape forging is preform location prior to the forging. Eccentric loading of preforms may results

*Corresponding author email: saranjitkiit@gmail.com

into off-centre loading, distortion of the preform and increased cavity filling loads. Thus, in net-shape forging, the filling of die cavities to a predetermined degree is of paramount importance, as it significantly affects the dimensional accuracy of the final components, forging load and tool stresses (Hou, 1997; Fereshteh-Saniee and Jaafari, 2002; Zhaoa *et al*., 2002; Samolyk and Pater, 2005). The present paper aims at studying this net-shape forging using sintered preforms as starting material.

Sinter-forging technology uses pressed and sintered metal powder preforms as starting material for the manufacture of precision engineering components virtually without scrap and combines the advantages associated with the powder metallurgy and conventional forging. The mechanical and metallurgical properties of sinter-forged components compare favorably with those of wrought materials and finds extensive applications in automobile, aerospace and defense industries (Jha and Kumar, 1983; Jha and Kumar, 1994; Frantsevic, 2000; Singh *et al*., 2001a; Ilia *et al*., 2005).

The net-shape forging is an extremely complex process from the point of view of deformation characteristics due to unsteady state and non-uniform metal flow along the die constraints. It is well-investigated fact that close control of preform volume, preheat temperature (if the process is not performed at room temperature), lubrication and the positioning of the preforms is absolutely necessary, if consistent components, safe loads and tool stresses are to be maintained. The non-uniformity in density distribution and complex die-workpiece-container interfacial friction conditions during processing of sintered materials further makes this process difficult to analyze (O'Connell *et al*., 1996; Majerus *et al*., 1997). The investigations into the various aspects of closed-die forging using conventional wrought materials have been reported by various researchers (Kwan, 2000; Hwang *et al*., 2001; Sljapic *et al*., 2002; Kwan, 2002; Malayappan and Narayanasamy, 2003; Bhutta and Chitkara, 2007) but very few have carried out the investigations of sinter-forging process (Jha and Kumar, 1996; Sutradhar and Gadkhindi, 1997; Sutradhar *et al*., 1997; Singh *et al*., 2001b; Cho *et al*., 2001; Huang and Cheng, 2002; Singh *et al*., 2002; Satsangi *et al*., 2003; Singh *et al*., 2003; Singh *et al*., 2004; Huang and Cheng, 2004; Justino *et al*., 2004; Jha and Gupta, 2005; Huang and Cheng, 2005; Yang and Hsua, 2006; Alves *et al*., 2006; Singh *et al*., 2006; Singh *et al*., 2007a; Singh *et al*., 2007b) and as such no work has been reported on the flashless net-shape forging of sintered materials.

In the present paper, the complete deformation of cylindrical preforms into double-hub-flange components has been considered in two subsequent stages, namely free barreling and constraint deformation. Also, three separate cases of deformation modes have been considered based on the division of preform into dead and deforming zones. Each deforming zones for all the modes have been analyzed based on *'Upper Bound'* approach and generalized expressions for the velocity field, strain rates, internal, frictional shear and inertia energy dissipations have been formulated. The theoretical analysis is based on the compatibility conditions and composite interfacial frictional shear equations already derived by the author (Singh *et al*., 2007c; Singh *et al*., 2008). The average die loads have been computed separately for all the deformation modes, when die cavity impressions were just about to be filled completely, *i.e.* an infinitesimal small corner filling was still left unfilled. The experiments have been performed on a hydraulic press using closed-die set having upper and lower counter punches with centrally located cylindrical recess cavities with diameter equal to that of the cylindrical preforms, so that preforms can be located centrally with respect to the central container. Both the theoretical and experimental results were compared and investigated critically. The effect of die velocity, preform aspect ratio on energy dissipations, die cavity fills and die loads have been investigated and results for the deformation modes have been compared. The effect of die speed *i.e.* dynamic effects has been investigated using inertia and load factors. It is expected that the present work will be useful for the analysis of net-shape forging of sintered materials.

UPPER BOUND ANALYSIS

The process of net-shape sinter-forging of cylindrical preform into double-hub flange component is performed by placing the preform within the two rigid closed die-halves comprising of upper punch, counter lower punch and container as shown in figure 1. The dies have cylindrical recess-cavities with depth and diameter equal to length and diameter of hubs. These cavities minimize the difficulty and variability during billet location within the closed-dies as discussed earlier. In the present paper, the complete deformation of cylindrical preforms into double-hub-flange components has been considered in two subsequent stages as shown in figure 2. The first stage consists of preform free vertical surface barreling till it touches the middle of the container sidewalls and the subsequent second stage consists of constrained deformation of bulged preform, where corners are formed and filled (approximated with straight dotted lines). The present theoretical analysis considers following assumptions (Jha and Kumar, 1997):

a) The circumferential flow of preform *i.e.* rotation of specimen is neglected.
b) The average die load is estimated at the end of forging operation when the load is maximum.
c) The barreling of preform during second phase, *i.e.* constraint deformation is neglected and the inclined surface of deforming preform remains inclined

during the entire die filling process.

d) The die-workpiece-container interfacial friction condition is assumed to be composite in nature and consists of both sliding and sticking frictions (Jha and Kumar, 1994) and the interfacial frictional shear equation is given in equation (1):

$$\tau = \mu\left\{P_{av} + \rho_0\phi_0\left[1-\left(\frac{r_m - r}{nR_0}\right)\right]\right\} \quad (1)$$

e) The relative density of preform varies during deformation, as compaction and compression takes place simultaneously (Jha and Kumar, 1986; Tabata and Masaki, 1978), thus compatibility equation is formulated accordingly as given in equation (2):

$$\dot{\varepsilon}_{rr} + \dot{\varepsilon}_{\theta\theta} + \left(\frac{1-2\eta}{1+\eta}\right)\dot{\varepsilon}_{zz} = 0 \quad (2)$$

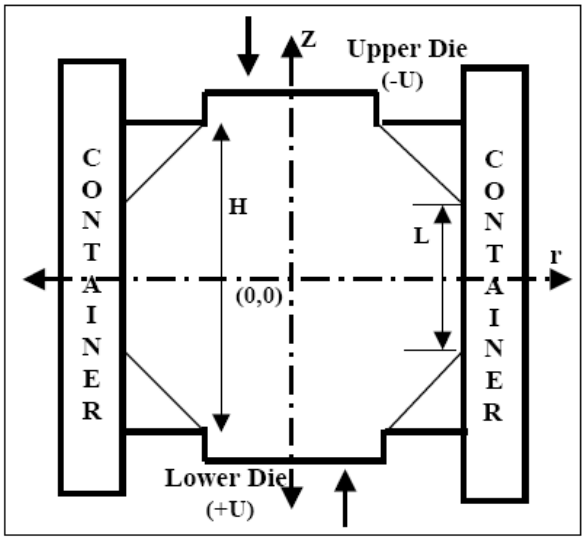

Fig. 1. Net-shape closed-die sinter-forging process.

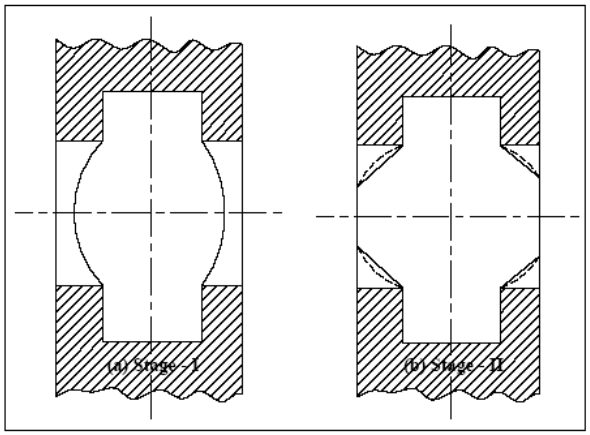

Fig. 2. Deformation stages during net-shape closed-die sinter-forging.

Three different deformation modes have been considered based on the different divisions of the preform into dead and deforming zones, which are discussed as deformation modes I, II and III. In all the three deformation modes, the quarter portion of deforming preform has been considered and divided into various zones. The total energy dissipation (Avitzur, 1968) expressed as sum of the various energy dissipations as given in equation (3) are formulated using boundary conditions, exponential velocity field and corresponding strain rates for these zones [Refer Appendix] and then summed to get the total energy dissipation separately for each of the deformation modes.

$$J = (W_i + W_f + W_a) = \left(\frac{2\sigma_o}{\sqrt{3}}\int_V \sqrt{\frac{1}{2}\dot{\varepsilon}_{ij}\dot{\varepsilon}_{ij}}\,dV + \int_S \tau|\Delta U|dS + \int_V \rho_i(a_i U_i)dV\right) \quad (3)$$

In case of deformation mode-I, the quarter portion of deforming preform have been divided into zones 1, 2 and 3, where zone 1 and 3 are dead and metal flow is considered in zone 2 only as shown in figure 3. In case of deformation mode-II, it has been divided into zones 1, 2, 3 and 4, where zone 1 is dead and metal flow is considered in zones 2, 3 and 4 as shown in figure 4. In case of deformation mode-III, it has been divided into zones 1, 2, 3, 4 and 5, where zone 1 and 3 are dead and metal flow is considered in zones 2, 4 and 5 as shown in figure 5. The corresponding equations for internal energy, frictional shear energy and inertia energy dissipations are formulated and shown below.

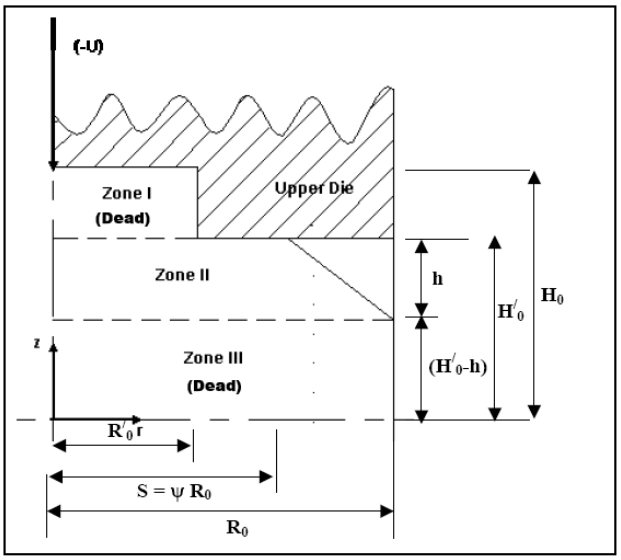

Fig. 3. Deformation Mode I.

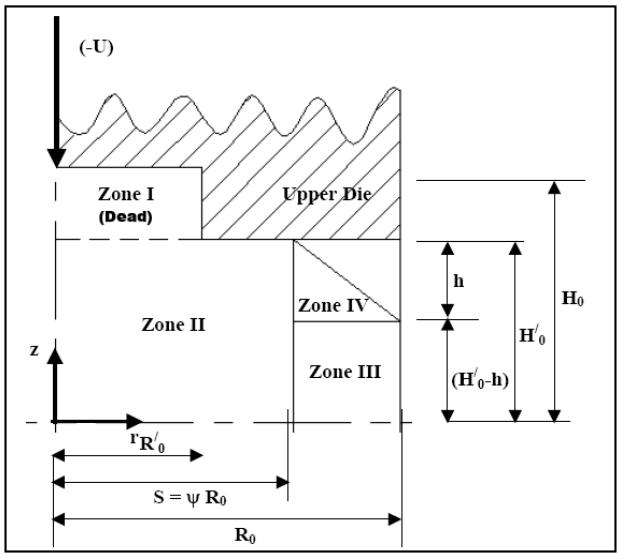

Fig. 4. Deformation Mode II.

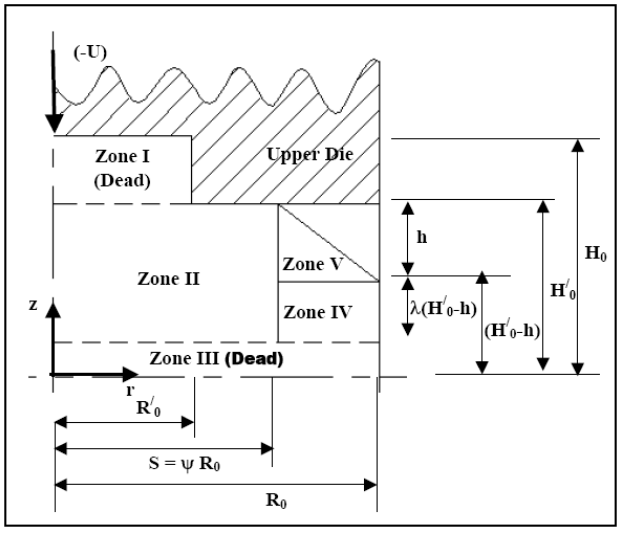

Fig. 5. Deformation Mode III.

Deformation Mode – I

Zone 1 & 3: Dead

Zone 2:

$$W_i = \left[\frac{\sqrt{2}\pi\sigma_0 U R_0^2 (2\psi+1)\alpha^{1/2}}{3\sqrt{3}(\alpha-2)^{1/2}} \right] \tag{4}$$

$$W_{f_1} = \left\{ \left[\frac{\pi\mu(1-2\eta)UR_0^3(\psi^3-\lambda^3)}{3(1+\eta)h} \right] \times \left[P_{av} + \rho_0\phi_0\left(1-\frac{r_m}{n\alpha R_0}\right) + \left(\frac{3\rho_0\phi_0}{4n\alpha}\right)\left(\frac{\psi^4-\lambda^4}{\psi^3-\lambda^3}\right) \right] \right\} \tag{5}$$

$$W_{f_2} = \left\{ \left(\frac{\pi\mu R_0 (H'_0-h)^2 U}{h} \right) \times \left\{ P_{av} + \rho_0\phi_0\left(1-\frac{z_m}{nH'_0}\right) + \left[\frac{2\rho_0\phi_0(H'_0-h)}{3nH'_0} \right] \right\} \right\} \tag{6}$$

$$W_a = \left\{ \left(\frac{\pi\rho_i(1-\psi)R_0^2 U}{10} \right) \left\{ \left[\frac{R_0^2(4\psi^3+3\psi^2+2\psi+1)U^2}{(\alpha-2)^{3/2}h^2} \right] + \left[\frac{(1+4\psi)U^2}{3} \right] + \left[\frac{20h(2\psi+1)\dot{U}}{1-\psi} \right] \right\} \right\} \tag{7}$$

Deformation Mode – II

Zone 1: Dead

Zone 2:

$$W_i = \left[\frac{\sqrt{2}\pi\sigma_0 R_0^2 \psi^2 U \alpha^{1/2}}{\sqrt{3}(\alpha-2)^{1/2}} \right] \tag{8}$$

$$W_{f_1} = \left\{ \left[\frac{\pi\mu(1-2\eta)UR_0^3(\psi^3-\lambda^3)}{3(1+\eta)H'_0} \right] \times \left\{ P_{av} + \rho_0\phi_0\left(1-\frac{r_m}{n\alpha\psi R_0}\right) + \left\{ \left(\frac{3\rho_0\phi_0}{4n\alpha\psi}\right)\left[\frac{\psi^4-\lambda^4}{\psi^3-\lambda^3}\right] \right\} \right\} \right\} \tag{9}$$

$$W_{f_2} = 0 \tag{10}$$

$$W_a = \left\{ \left(\frac{\pi\rho_i\psi^2 R_0^2 U}{3} \right) \times \left\{ \left[\frac{3(1-2\eta)^3\psi^2 R_0^2}{16(1+\eta)^3 H_0'^2} - 1 \right] U^2 + 3\dot{U}H'_0 \right\} \right\} \tag{11}$$

Zone 3:

$$W_i = \left[\frac{\sqrt{2}\pi\sigma_0 (H'_0-h)^2 R_0^2 (1-\psi)^2 U \alpha^{1/2}}{\sqrt{3}H_0'^2(\alpha-2)^{1/2}} \right] \tag{12}$$

$$W_{f_1} = 0 \tag{13}$$

$$W_{f_2} = \left\{ \left(\frac{\pi\mu R_0 (H'_0-h)^3 U}{H_0'^2} \right) \times \left\{ p_{av} + \rho_0\phi_0\left(1-\frac{z_m}{nH'_0}\right) + \left[\frac{2\rho_0\phi_0(H'_0-h)}{3nH'_0} \right] \right\} \right\} \tag{14}$$

$$W_a = \left\{ \left[\frac{\pi\rho_i R_0^2(1-\psi^2)U}{3} \right] \times \left\{ \left[\frac{3(1-2\eta)^3 R_0^2(1+\psi^2)}{16(1+\eta)^3(H'_0-h)^2} - 1 \right] \times \left(\frac{H'_0-h}{H'_0} \right)^6 U^2 + 3\dot{U}(H'_0-h) \right\} \right\} \tag{15}$$

Zone 4:

$$W_i = \left[\frac{\pi\sigma_0 (2H'_0-h) R_0^2 (4-\psi-7\psi^2) U \alpha^{1/2}}{3\sqrt{6}H'_0(\alpha-2)^{1/2}} \right] \tag{16}$$

$$W_{f_1} = W_{f_2} = 0 \tag{17}$$

$$W_a = \left\{ \left[\frac{\pi\rho_i(1-\psi)R_0^2(2H'_0-h)^3 U^3}{6H_0'^3} \right] \times \left\{ \left[\frac{(3\psi^3+3\psi^2+\psi-1)R_0^2}{(\alpha-2)^{3/2}h^2} \right] + \frac{6hH'_0(2\psi+1)\dot{U}}{(2H'_0-h)U^2} \right\} \right\} \tag{18}$$

Deformation Mode – III

Zone 1 & 3: Dead

Zone 2:

$$W_i = \left[\frac{\sqrt{2}\pi\sigma_0 R_0^2 \psi^2 U \alpha^{1/2}}{\sqrt{3}(\alpha-2)^{1/2}} \right] \tag{19}$$

$$W_{f_1} = \left\{ \left[\frac{\pi\mu(1-2\eta)UR_0^3(\psi^3-\lambda^3)}{3(1+\eta)\left[(1-\lambda)h+\lambda H'_0\right]} \right] \times \left\{ P_{av} + \rho_0\phi_0\left(1-\frac{r_m}{n\alpha\psi R_0}\right) + \left\{ \left(\frac{3\rho_0\phi_0}{4n\alpha\psi}\right)\left[\frac{\psi^4-\lambda^4}{\psi^3-\lambda^3}\right] \right\} \right\} \right\} \tag{20}$$

$$W_{f_2} = 0 \tag{21}$$

$$W_a = \left\{ \left(\frac{\pi\rho_i\psi^2 R_0^2 U}{3} \right) \times \left\{ \left[\frac{3(1-2\eta)^3\psi^2 R_0^2}{16(1+\eta)^3\left[(1-\lambda)h+\lambda H_0'^2\right]^2} - 1 \right] U^2 + 3\dot{U}\left[(1-\lambda)h+\lambda H_0'^2\right] \right\} \right\} \tag{22}$$

Zone 4:

$$W_i = \left[\frac{\sqrt{2}\pi\sigma_0\lambda^2 (H'_0-h)^2 R_0^2 (1-\psi^2) U \alpha^{1/2}}{\sqrt{3}\left[(1-\lambda)h+\lambda H'_0\right]^2(\alpha-2)^{1/2}} \right] \tag{23}$$

$$W_{f_1} = 0 \tag{24}$$

$$W_{f_2} = \left\{ \left(\frac{\pi\mu R_0\lambda^3 (H'_0-h)^3 U}{\left[(1-\lambda)h+\lambda H'_0\right]^2} \right) \times \left\{ p_{av} + \rho_0\phi_0\left(1-\frac{z_m}{nH'_0}\right) + \left[\frac{2\rho_0\phi_0\lambda(H'_0-h)}{3nH'_0} \right] \right\} \right\} \tag{25}$$

$$W_a = \left\{ \left[\frac{\pi\rho_i R_0^2(1-\psi^2)U}{3} \right] \times \left\{ \left[\frac{3(1-2\eta)^3 R_0^2(1+\psi^2)}{16(1+\eta)^3\lambda^2(H'_0-h)^2} - 1 \right] \times \left[\frac{\lambda^6(H'_0-h)^6}{\left[(1-\lambda)h+\lambda H'_0\right]^6} \right] U^2 + 3\dot{U}\lambda(H'_0-h) \right\} \right\} \tag{26}$$

Zone 5:

Table 1. Physical and chemical characteristics of the aluminium metal powder.

Particle size (μ)	Weight Under (%)	Chemical Analysis	Weight (%)
118.0	100.0	Aluminium	99.500
88.1	98.9	Iron	< 0.1700
65.6	95.5	Silicon	< 0.1313
48.8	88.8	Zinc	< 0.0053
36.3	79.0	Manganese	< 0.0023
27.0	65.8	Magnesium	< 0.0016
17.4	40.1	Apparent density	1.25 gm/cc
13.0	25.5	Tap density	1.50 gm/cc

$$W_i = \left[\frac{\pi\sigma_0\chi R_0^2 U\alpha^{1/2}}{3\sqrt{6}(\alpha-2)^{1/2}}\right] \quad (27)$$

$$W_{f_1} = W_{f_2} = 0 \quad (28)$$

$$W_a = \left[\frac{\pi\rho_i(1-\psi)R_0^2U^3}{6}\right]\times\left\{\left[\frac{3\chi^3R_0^2\left[\left(4\psi^4+3(\psi^2+1)(\psi-1)\right)\right]}{(\alpha-2)^{3/2}(1-\psi)}\right]+\frac{2R_0\chi^3(2\psi+1)(1-3\chi)}{h}+\frac{2\dot{U}h(2\psi+1)}{U^2}\right\} \quad (29)$$

where, $\psi = \left(\frac{S}{R_0}\right)$, $\lambda = \left(\frac{R_0'}{R_0}\right)$, $\alpha = \left\{2+\left[\frac{2(1+\eta)}{1-2\eta}\right]^2\right\}$ and

$$\chi = \left[2+\frac{h}{\lambda(H_0'-h)}\right]$$

The total energy dissipations and subsequently the average die load for both the deformation modes may be computed by substituting equations (4) to (29) into equations (30) and (31) respectively as:

$$J = 4\sum_j \left(W_i + W_{f_1} + W_{f_2} + W_a\right)_j \quad (30)$$

where, '*j*' is number of zones

$$F_{av} = J(U)^{-1}A_{av} \quad (31)$$

EXPERIMENTAL WORK

To investigate the deformation mechanism during present net-shape closed-die sinter-forging process, experiments were conducted on the sintered aluminium cylindrical preforms fabricated by compacting the aluminium metal powder in a graphite lubricated compaction dies having bore diameter equal to 30 mm at recorded compacting pressure of about 15-20 tonf. Table 1 shows the physical and chemical characteristics of the aluminium metal powder used for the preform fabrication. The green compacts were sintered at about 400 ^{0}C for four hours in an endothermic sand atmosphere and were finally machined and polished to the required dimensions. The densities of preforms were obtained by measuring their dimensions and weights and the corresponding relative densities were obtained by taking the ratio of density of preform to that of the density of solid metal. The final experiments of the net-shape closed-die forging of sintered preforms were conducted on a 150-ton hydraulic press using closed-die sets as shown in figure 6. The preforms having different shape complexity factors were forged at dry and lubricated interfacial friction conditions and corresponding strains (axial and radial), as well as forging load were recorded to investigate the dynamic effects. Figure 7 shows some of the deformed cylindrical preforms.

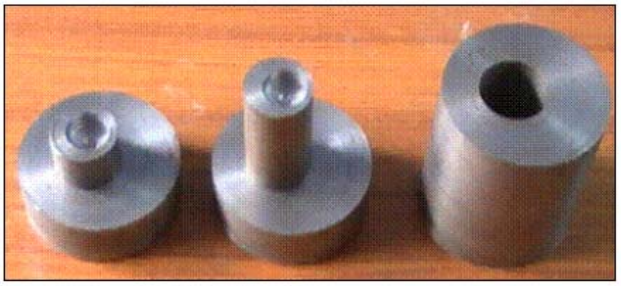

Fig. 6. Closed-die Set.

Fig. 7. Deformed Preforms.

RESULTS AND DISCUSSION

A typical data of preform and deformation characteristics has been considered as:

R_0 = 15 mm; R_0' = 10 mm; H_0 = 20 mm; ψ = 0.80; $\rho_0\phi_0$ = 0.30 P_{av}; σ_0 = 6.25 kg/mm^2; ρ_i = 2 × 10^3 kg/m^3; n = 2; ρ_0 = 0.75; (H_0' / R_0) = 0.25 to 1.0 and U = 0.01 – 0.2 m/sec.

The variation in height reduction with die velocity for various preform aspect ratios has been displayed in figure 8. It is evident that preform height reduction increases with die velocity and also preforms with higher aspect

ratio exhibits higher height reduction. Thus, slender preform deforms comparatively more than shorter preform under same die load during uniaxial compression. The change in relative density with corresponding die load has been displayed in figure 9 and it is found to increase with die load and die-cavity fills, as preform material flows along the container and die-wall constraints. The densification is also better for higher die velocity. Figure 10 shows the variation of inertia factor 'ξ' (ratio of inertia energy dissipated to total external energy supplied by press die platens) with die velocity and it is found to increase exponentially with die velocity and preform aspect ratio. Also, it is higher for deformation mode I. Thus, for closed-die sinter-forging operations, especially at higher die velocity, the magnitude of inertia energy dissipation is comparable to other energy dissipations and must be considered during analysis.

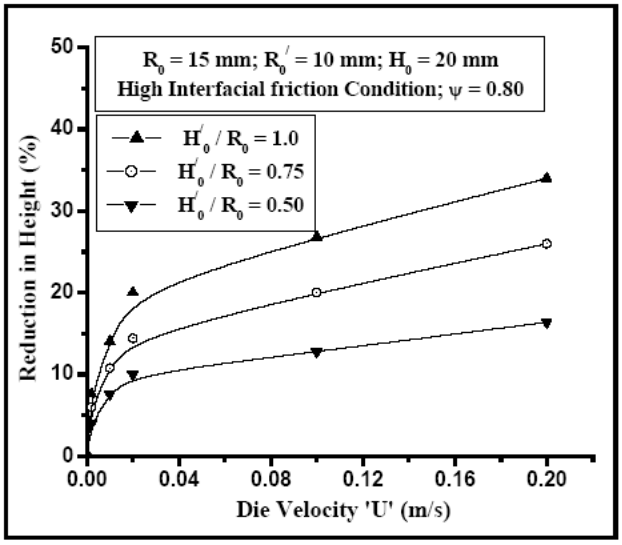

Fig. 8. Variation of height reduction with die velocity.

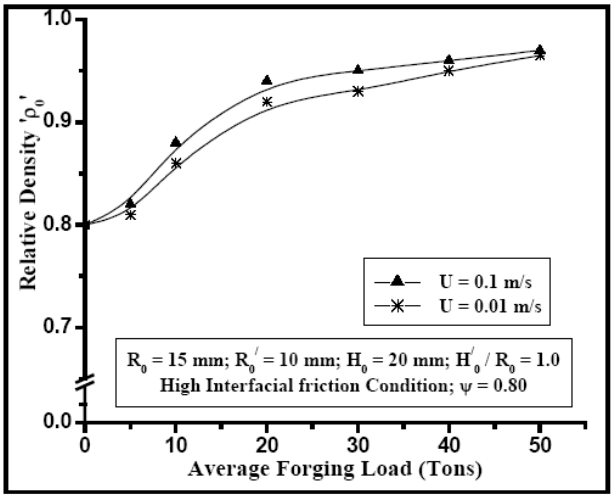

Fig. 9. Variation of relative density with average forging load.

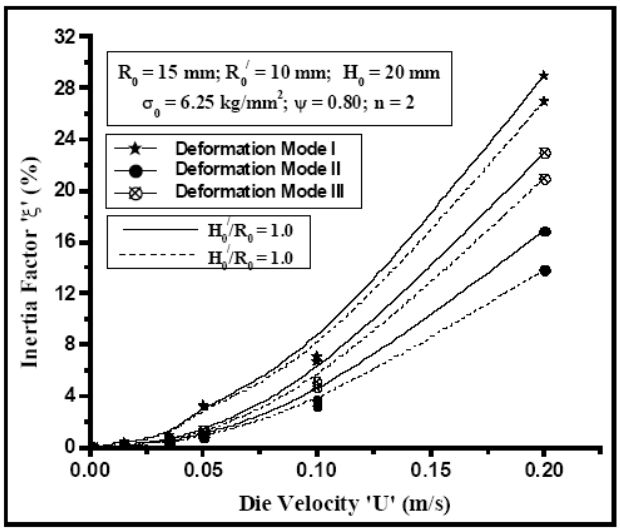

Fig. 10. Variation of inertia factor with die velocity.

Figure 11 shows variation of average forging load with the ratio of unfilled die volume to component's volume for various aspect ratios and die velocity. It is apparent that load is exponentially high at the final stages of die filling operation due to high constraint deformation and resistance against metal flow. The load curves are also high for higher preform aspect ratio due to two prominent reasons. First, the geometry of corners differs with preform aspect ratio, due to difference in barreling during free upsetting stage of deformation. Second, the preform with lower aspect ratio has lower contact area with container walls, resulting into low friction shear energy dissipations. The variation of load factor 'ζ' (ratio of difference in average die load with and without dynamic effects to average die load with dynamic effects) is shown in figure 12. It decreases rapidly and become asymptote with x-axis at higher die velocity. This is attributed due to shorter contact time under deformation, which does not

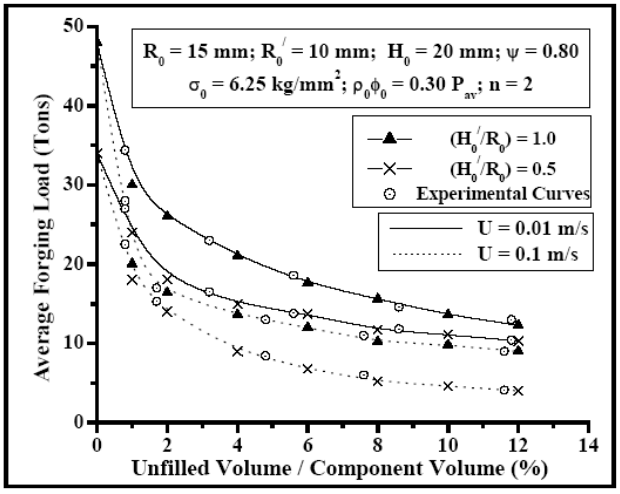

Fig. 11. Variation of forging load with ratio of unfilled die volume to component's volume.

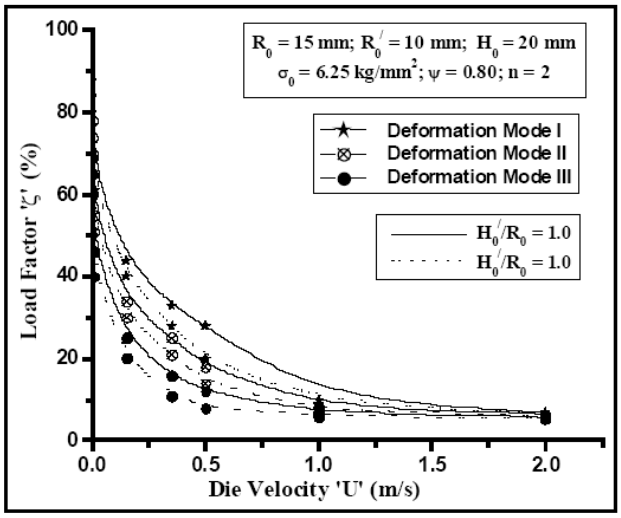

Fig. 12. Variation of load factor with die velocity.

allows the internal heat generated during deformation to escape quickly and hence, decreases the resistance of preform material. Also, load requirement under deformation mode-I is higher than deformation mode-II and thus, it is more effective for predicting the forging load requirement for complete die-fill during flashless closed-die sinter-forging of double-hub flange component.

CONCLUSIONS

- The inertia energy dissipation increases exponentially with die velocity and its magnitude becomes comparable to other energy dissipations at higher die velocity, which has been has been illustrated using an inertia factor 'ξ'. Therefore, it must be considered during analysis of sinter-forging operations for accurate and reasonable measure of die load.
- The die load decreases with die velocity, which has been demonstrated using load factor 'ζ'. The die load increases exponentially with the die cavity fills during complete filling stage *i.e.* forcing of sintered materials into the cavities of impressions. This is because sinter-forging operations at higher die speeds are characterized by very small contact time under load, which restricts the internal heat generated during plastic working to dissipate quickly and hence, reduces the resistance of sintered materials against deformation.
- The deformation mode-I gives higher estimate of die load, as compared to the deformation mode-II due to larger dead zones and higher squeezing effect of sintered material into cavities of impression. Hence, deformation mode-I is more effective for predicting the die load requirements for complete die fills and must be preferred during design process also.
- The preforms with high aspect ratio *i.e.* slender preforms deform at higher die loads and exhibit higher change in height, as compared to the shorter preforms. This is due to two prominent reasons, first, due to the difference in geometry of the unfilled die corners *i.e.* difference in barreling for various preform aspect ratios. Secondly, the slender preforms make contact with die container walls earlier and the contact area is large for same die load, as compared to the shorter preforms, leading to high interfacial friction shear energy dissipations.

It is expected that the present research work will be highly useful carrying further research work in the field of flashless closed-die forging of sintered preforms.

APPENDIX

The boundary conditions, velocity field, strain rates for zone-2 of the deformation mode – I are:

Zone - 2

Boundary Conditions

$U_z = 0$ at $z = (H_0' - h)$ (1a)

$U_z = -U$ at $z = H_0'$ (2a)

Velocity Field

$$U_r = \left[\frac{(1-2\eta)Ur}{2(1+\eta)h}\right] \quad (3a)$$

$$U_z = -\left[\frac{z-(H_0'-h)}{h}\right]U \quad (4a)$$

$$U_\theta = 0 \quad (5a)$$

Strain Rates

$$\dot{\varepsilon}_{rr} = \dot{\varepsilon}_{\theta\theta} = \left[\frac{(1-2\eta)U}{2(1+\eta)h}\right] \quad (6a)$$

$$\dot{\varepsilon}_{zz} = -\left(\frac{U}{h}\right) \quad (7a)$$

$$\dot{\varepsilon}_{r\theta} = \dot{\varepsilon}_{\theta z} = \dot{\varepsilon}_{rz} = 0 \quad (8a)$$

The boundary conditions, velocity field, strain rates for zones-2, 3 & 4 of the deformation mode – II are:

Zone 2

Boundary Conditions

$U_z = -U$ at $z = H_0'$ (9a)

$U_z = 0$ at $z = 0$ (10a)

Velocity Field

$$U_r = \left[\frac{(1-2\eta)Ur}{2(1+\eta)H_0'}\right] \quad (11a)$$

$$U_z = -\left(\frac{Uz}{H_0'}\right) \quad (12a)$$

$$U_\theta = 0 \quad (13a)$$

Strain Rates

$$\dot{\varepsilon}_{rr} = \dot{\varepsilon}_{\theta\theta} = \left[\frac{(1-2\eta)U}{2(1+\eta)H_0'}\right] \quad (14a)$$

$$\dot{\varepsilon}_{zz} = -\left(\frac{U}{H'_0}\right) \quad (15a)$$

$$\dot{\varepsilon}_{r\theta} = \dot{\varepsilon}_{\theta z} = \dot{\varepsilon}_{rz} = 0 \quad (16a)$$

Zone 3

Boundary Conditions

$U_z = 0$ at $z = 0$ (17a)

$U_z = -U\,[(H'_0\text{-}h)/H'_0]$ at $z = (H'_0 - h)$ (18a)

Velocity Field

$$U_r = \left[\frac{(1-2\eta)Ur}{2(1+\eta)H'_0}\right] \quad (19a)$$

$$U_z = -\left[\frac{Uz}{H'_0}\right] \quad (20a)$$

$$U_\theta = 0 \quad (21a)$$

Strain Rates

$$\dot{\varepsilon}_{rr} = \dot{\varepsilon}_{\theta\theta} = \left[\frac{(1-2\eta)U}{2(1+\eta)H'_0}\right] \quad (22a)$$

$$\dot{\varepsilon}_{zz} = -\left[\frac{U}{H'_0}\right] \quad (23a)$$

$$\dot{\varepsilon}_{r\theta} = \dot{\varepsilon}_{\theta z} = \dot{\varepsilon}_{rz} = 0 \quad (24a)$$

Zone 4

Boundary Conditions

$U_z = -U\,[(H'_0\text{-}h)/H'_0]$ at $z = (H'_0 - h)$ (28a)

$U_z = -U$ at $z = H'_0$ (29a)

Velocity Field

$$U_r = \left[\frac{(1-2\eta)Ur}{2(1+\eta)H'_0}\right] \quad (30a)$$

$$U_z = -\left[\frac{Uz}{H'_0}\right] \quad (31a)$$

$$U_\theta = 0 \quad (32a)$$

Strain Rates

$$\dot{\varepsilon}_{rr} = \dot{\varepsilon}_{\theta\theta} = \left[\frac{(1-2\eta)U}{2(1+\eta)H'_0}\right] \quad (33a)$$

$$\dot{\varepsilon}_{zz} = -\left[\frac{U}{H'_0}\right] \quad (34a)$$

$$\dot{\varepsilon}_{r\theta} = \dot{\varepsilon}_{\theta z} = \dot{\varepsilon}_{rz} = 0 \quad (36a)$$

The boundary conditions, velocity field, strain rates for zones-2, 4 & 5 of the deformation mode – III are:

Zone 2

Boundary Conditions

$U_z = 0$ at $z = [(H'_0 - h)(1-\lambda)]$ (37a)

$U_z = -U$ at $z = H'_0$ (38a)

Velocity Field

$$U_r = \left[\frac{1-2\eta}{2(1+\eta)}\right]\left[\frac{Ur}{H'_0 - (H'_0 - h)(1-\lambda)}\right] \quad (39a)$$

$$U_z = -\left[\frac{z-(H'_0-h)(1-\lambda)}{H'_0-(H'_0-h)(1-\lambda)}\right]U \quad (40a)$$

$$U_\theta = 0 \quad (41a)$$

Strain Rates

$$\dot{\varepsilon}_{rr} = \dot{\varepsilon}_{\theta\theta} = \left[\frac{1-2\eta}{2(1+\eta)}\right]\left[\frac{U}{H'_0 - (H'_0 - h)(1-\lambda)}\right] \quad (42a)$$

$$\dot{\varepsilon}_{zz} = -\left[\frac{U}{H'_0-(H'_0-h)(1-\lambda)}\right] \quad (43a)$$

$$\dot{\varepsilon}_{rz} = \dot{\varepsilon}_{r\theta} = \dot{\varepsilon}_{\theta z} = 0 \quad (44a)$$

Zone 4

Boundary Conditions

$U_z = 0$ at $z = [(H'_0 - h)(1-\lambda)]$ (45a)

$$U_z = -\left[\frac{U\lambda(H'_0-h)}{h+\lambda(H'_0-h)}\right] \text{ at } z = (H'_0 - h) \quad (46a)$$

Velocity Field

$$U_r = \left[\frac{1-2\eta}{2(1+\eta)}\right]\left[\frac{Ur}{h+\lambda(H'_0-h)}\right] \quad (47a)$$

$$U_z = -\left[\frac{z-(H'_0-h)(1-\lambda)}{h+\lambda(H'_0-h)}\right] \quad (48a)$$

$$U_\theta = 0 \quad (49a)$$

Strain Rates

$$\dot{\varepsilon}_{rr} = \dot{\varepsilon}_{\theta\theta} = \left[\frac{1-2\eta}{2(1+\eta)}\right]\left[\frac{U}{h+\lambda(H'_0-h)}\right] \quad (50a)$$

$$\dot{\varepsilon}_z = -\left[\frac{U}{h+\lambda(H'_0-h)}\right] \quad (51a)$$

$$\dot{\varepsilon}_{rz} = \dot{\varepsilon}_{r\theta} = \dot{\varepsilon}_{\theta z} = 0 \quad (52a)$$

Zone 5

Boundary Conditions

$$U_z = \left[\frac{\lambda(H'_0-h)}{h+\lambda(H'_0-h)}\right]U \text{ at } z = 0 \quad (53a)$$

$U_z = -U$ at $z = H'_0$ (54a)

Velocity Field

$$U_z = -\left[1-\frac{\chi z}{H'_0}\right]\left[\frac{U}{(\chi-1)}\right] \quad (55a)$$

$$U_r = \left[\frac{1-2\eta}{2(1+\eta)}\right]\left[\frac{\chi Ur}{(\chi-1)H'_0}\right] \quad (56a)$$

$$U_\theta = 0 \quad (57a)$$

Strain Rates

$$\dot{\varepsilon}_{rr} = \dot{\varepsilon}_{\theta\theta} = \left[\frac{1-2\eta}{2(1+\eta)}\right]\left[\frac{\chi U}{(\chi-1)h}\right] \quad (58a)$$

$$\dot{\varepsilon}_{zz} = -\left[\frac{\chi U}{(\chi-1)h}\right] \quad (59a)$$

$$\dot{\varepsilon}_{rz} = \dot{\varepsilon}_{r\theta} = \dot{\varepsilon}_{\theta z} = 0 \quad (60a)$$

REFERENCES

Alves, LMM. Martins, PAF. and Rodrigues, JMC. 2006. A New Yield Function for Porous Materials. Journal of Materials Processing Technology. 179(1-3):36-43.

Avitzur, B. 1968. Metal Forming Processes and Analysis. McGraw Hill, New York, USA.

Bhutta, MA. and Chitkara, NR. 2007. Dynamic Forging of Splines and Spur Gear Forms: A Modified Upper Bound Analysis that Includes the Effects of Inertia and Some Experiments. Journal of Materials Processing Technology. 191:372.

Cho, JR., Joo, YS. and Jeong, HS. 2001. The Al-Powder Forging Process: Its Finite Element Analysis. Journal of Materials Processing Technology. 111(1-3):204-209.

Fereshteh-Saniee, F. and Jaafari, M. 2002. Analytical, Numerical and Experimental Analyses of Closed-Die Forging. Journal of Materials Processing Technology. 125-126:334-340.

Frantsevic, IN. 2000. The Place of Powder Metallurgy in Contemporary Material Science and Technology. Powder Metallurgy and Metal Ceramics. 39(7-8):334-345.

Hou, J. 1997. A Plane-Strain UBET Analysis of Material Flow in a Filled Deep Die Cavity in Closed-Die Forging. Journal of Materials Processing Technology. 70:103-110.

Huang, CC. and Cheng, JH. 2002. Forging Simulation of Sintered Powder Compacts under various Frictional Conditions. International Journal of Mechanical Sciences. 44(3):489-507.

Huang, CC. and Cheng JH. 2004. An Investigation into the Forming Limits of Sintered Porous Materials under different Operational Conditions. Journal of Materials Processing Technology. 148(3):382-393.

Huang, CC. and Cheng, JH. 2005. A New Forming-Limit Criterion for Fracture Prediction in a Powder Forging Application. International Journal of Mechanical Sciences. 47(7):1123-1145.

Hwang, BC., Hong, SJ. and Bae, WB. 2001. An UBET Analysis of the Non-Axisymmetric Extrusion/Forging of Process. Journal of Materials Processing Technology. 111(1-3):135-141.

Ilia, E., Tutton, K. and O'Neill, M. 2005. Forging a Way towards a Better Mix of PM Automotive Steels. Metal Powder Report. 60(3):38-44.

Jha, AK. and Gupta, AK. 2005. Closed Die Forging of Powder Preforms. Journal of Production Engineering. The Institution of Engineers (India). 85:51-59.

Jha, AK. and Kumar, S. 1983. Forging of Metal Powder Preforms. International Journal of Machine Tool Design and Research. 23(4):201-212.

Jha, AK. and Kumar, S. 1986. Deformation Characteristics and Fracture Mechanisms during the Cold Forging of Metal Powder Preforms. International Journal of Machine Tool Design and Research. 26(4):369-384.

Jha, AK. and Kumar, S. 1994. Compatibility of Sintered Materials during Cold Forging. International Journal of Materials and Product Technology. 9:281-299.

Jha, AK. and Kumar, S. 1996. Dynamic Effects during High-Speed Sinter-Forging Process. International Journal of Machine Tool Design and Research. 36(10):1109-1112.

Jha, AK. and Kumar, S. 1997. Investigations into the High-Speed Forging of Sintered Copper Powder Strips. Journal of Materials Processing Technology. 71:394-401.

Jha, AK. Sutradhar, G. and Kumar, S. 1994. Production of Sinter-Forged Components. Journal of Materials Processing Technology. 41(2):143-169.

Justino, JG., Alves, MK., Klein, AN. and Al-Qureshi, HA. 2004. Constitutive Model for the Elastic-Plastic Analysis of Porous Sintered Materials. International Journal of Machine Tools and Manufacture. 44:1471-1479.

Kwan, CT. 2000. A Concave Circular Parallelepiped Element and its Applications to Three-Dimensional Closed-Die Forging. Journal of Materials Processing Technology. 123:203-208.

Kwan, CT. 2002. An Analysis of the Closed-Die Forging of a General Non-Axisymmetric Shape by the Upper-Bound Elemental Technique. Journal of Materials Processing Technology. 123:197-202.

Lee, JH., Kim, YH. and Bae, WB. 1997. A Study on Flash- and Flashless-Precision Forging by the Upper-Bound Elemental Technique. Journal of Materials Processing Technology. 72:371-379.

Majerus, JN., Jen, KP. and Gong, H. 1997. Qualitative Data for Precision, Closed-Die Forging via "Line-Averaged" Residual Plastic-Strains. International Journal of Machine Tools Manufacture. 37(4):523-554.

Malayappan, S. and Narayanasamy, R. 2003. Some Aspects on Barrelling in Aluminium Solid Cylinders during Cold Upset Forging using a Die with Constraints. Journal of Materials Processing Technology. 135:18-29.

O'Connell, M., Painter, B., Maul, G. and Altan, T. 1996. Flashless Closed-Die Upset Forging-Load Estimation for Optimal Cold Header Selection. Journal of Materials Processing Technology. 59:81-94.

Samolyk, G. and Pater, Z. 2005. Use of SLFET for Design of Flash Gap with V-Notched Lands in a Closed-Die Forging. Journal of Materials Processing Technology. 162-163:558-563.

Satsangi, PS., Sharma, PC. and Prakash, R. 2003. An Elastic-Plastic Finite Element Method for Analysis of Powder Metal Forging. Journal of Materials Processing Technology. 136(1-3):80-87.

Serdyuk, GG., Sakhnenko, AV. and Svistun, LI. 2000. Manufacturing of Powdered Metals, Economics and Production Organization: Industrial use of the High-Rate (Impact) Pressing of Metallic Powders. Powder Metallurgy and Metal Ceramics. 39(9-10):514-520.

Singh, S., Agrawal, M., Jha, AK. and Kumar, S. 2002. A Computer Simulation Technique to Estimate Die Load and Energy during Sinter-Forging Process. Journal of Production Engineering, Institution of Engineers (India). 83:27-33.

Singh, S., Jha SK., Jha, AK. and Kumar, S. 2008. Investigations into Heterogeneous Deformation of Sintered Preforms due to Die-Workpiece Interfacial Friction. Indian Journal of Tribology. 2(3):1-6.

Singh, S., Jha, AK. and Kumar, S. 2001[b]. Analysis of Dynamic Effects during High-Speed Forging of Sintered Preforms. Journal of Materials Processing Technology. 112:53-62.

Singh, S., Jha, AK. and Kumar, S. 2004. An Energy Analysis during Forging of Sintered Truncated Conical Preform at High-Speed. Tamkang Journal of Science and Engineering. 7(4):227-236.

Singh, S., Jha, AK. and Kumar, S. 2006. Forging of Sintered Components: Technology Management Issues. Journal of Manufacturing Technology Today, CMTI. 2(5):23-27.

Singh, S., Jha, AK. and Kumar, S. 2007[a]. Dynamic Effects during Sinter-Forging of Axi-Symmetric Hollow Disc Preforms. International Journal of Machine Tools Manufacture. 47: 1101-1113.

Singh, S., Jha, AK. and Kumar, S. 2007[b]. Upper Bound Analysis & Experimental Investigations of Dynamic Effects during Sinter-Forging of Irregular Polygonal Preforms. Journal of Materials Processing Technology. 194:134-144.

Singh, S., Jha, AK. and Kumar, S. 2007[c]. High-Speed Sinter-Forging of Annular Ring Component. Tamkang Journal of Science and Engineering. 10(1):1-12.

Singh, S., Jha, SK., Jha, AK. and Kumar, S. 2003. Frictional Conditions during Sinter-Forging. Journal of Manufacturing Technology Today, CMTI. 2(10):12-16.

Singh, S., Singh, RK., Jha, AK. and Kumar, S. 2001[a]. Sintered Preforms Adds Better Value to Aerospace Components. Journal of Aerospace Engineering, Institution of Engineers (India). 82:1-6.

Sljapic, V., Hartley, P. and Pillinger, I. 2002. Observations on Fracture in Axi-Symmetric and Three-Dimensional Cold Upsetting of Brass. Journal of Materials Processing Technology. 125-126:267-274.

Sutradhar, G. and Gadkhindi, MM. 1997. Axisymmetric Closed Die Forging of Aluminium Powder Components. Metal Powder Report. 52(3):43.

Sutradhar, G., Bashashwan, AA., Jha, AK. and Kumar, S. 1997. Closed Die Axisymmetric Forging of Sintered Aluminium Preforms. Journal of Materials Processing Technology. 68:19-22.

Tabata, T. and Masaki, M. 1978. A Yield Criterion for Porous Metals and Analysis of Axial Compression of Porous Discs. Memories of Osaka Institution of Technology, Series-B, Science and Technology. 22(2):45-56.

Thomson, PF. 1986. Densification of Sintered Metal Compacts by Cold Deformation. Journal of Mechanical Working Technology. 13(2):219-227.

Yang, T. and Hsua, Y. 2006. Study on the Bulging Deformation of the Porous Metal in Upsetting. Journal of Materials Processing Technology. 177(1-3):154-158.

Zhaoa, G. Wang, G. and Grandhi, RV. 2002. Die Cavity Design of Near Flashless Forging Process using FEM-based Backward Simulation. Journal of Materials Processing Technology. 121:173-181.

Received: June 17, 2010; Revised and Accepted: Dec 15, 2010